arXiv:1408.4913v1 [cond-mat.dis-nn] 21 Aug 2014

FIRST PRINCIPLES STUDY OF A SODIUM BOROSILICATE GLASS-FORMER I: THE LIQUID STATE

Laurent Pedesseau,* Simona Ispas,† and Walter Kob‡
Laboratoire Charles Coulomb, UMR 5221, Université Montpellier 2 and CNRS, 34095 Montpellier, France

We use *ab initio* simulations to study the static and dynamic properties of a sodium borosilicate liquid with composition $3Na_2O$-B_2O_3-$6SiO_2$, i.e. a system that is the basis of many glass-forming materials. In particular we focus on the question how boron is embedded into the local structure of the silicate network liquid. From the partial structure factors we conclude that there is a weak nanoscale phase separation between silicon and boron and that the sodium atoms form channel-like structures as they have been found in previous studies of sodo-silicate glass-formers. Our results for the X-ray and neutron structure factor show that this feature is basically unnoticeable in the former but should be visible in the latter as a small peak at small wave-vectors. At high temperatures we find a high concentration of three-fold coordinated boron atoms which decreases rapidly with decreasing T, whereas the number of four-fold coordinated boron atoms increases. Therefore we conclude that at the experimental glass transition temperature most boron atoms will be four-fold coordinated. We show that the transformation of $^{[3]}$B into $^{[4]}$B with decreasing T is not just related to the diminution of non-bridging oxygen atoms as claimed in previous studies, but to a restructuration of the silicate matrix. The diffusion constants of the various elements show an Arrhenius behavior and we find that the one for boron has the same value as the one of oxygen and is significantly larger than the one of silicon. This shows that these two network formers have rather different dynamical properties, a result that is also confirmed from the time dependence of the van Hove functions. Finally we show that the coherent intermediate scattering function for the sodium atoms is very different from the incoherent one and that it tracks the one of the matrix atoms.

I. INTRODUCTION

Borosilicate glasses have many remarkable properties such as a low thermal expansion coefficient, weak electrical conductivity, high resistance to thermal shocks, and good stability regarding corrosion [1, 2]. Thanks to these features, these glasses have widespread applications going from every-day kitchenware to laboratory glassware, from insulating materials to those used for immobilisation of the nuclear waste [3–6]. The borosilicates that are of technological interest contain, apart from silicon and boron oxides, also a certain amount of network modifiers such as alkali and alkaline-earth oxides, as well as network formers such as Al or P. It is the resulting complex structure that is believed to give these glasses their remarkable properties [1] and hence understanding this structure poses also an interesting challenge for fundamental science.

One possibility to gain insight how the distinctive features of these glasses are related to their composition is to study a series of simple compositions, e.g. the ternary alkali borosilicates M_2O-B_2O_3-SiO_2, with M=Li, Na, K. Despite the apparent simplicity of these alkali borosilicates, they present non trivial physical and chemical behavior under a change of composition, temperature, pressure, or irradiation and hence such comparative studies have allowed to understand some of the connections between structure and properties [7–16]. These kind of studies have demonstrated the need to obtain quantitative information on the factors responsible for the properties that make these materials so important for glass technology, and in order to achieve this goal it has become mandatory to understand their structure on the atomistic scale. Hence, one needs an answer to the simple but probably the most fundamental question: How does boron modify the structure/integrate into the silica network? Answering this question will help to design new compositions that are energy- and environmentally-friendly and hence needed to make progress in the field.

In the late seventies and early eighties of the 20^{th} century, several studies have been carried out for the ternary composition containing sodium oxide, i.e. Na_2O-B_2O_3-SiO_2. Many of these studies were done by Yun, Bray, Dell and co-workers, using solid-state nuclear magnetic resonance spectroscopy (NMR) [17–19] of ^{11}B. Based on these experiments, a structural model has been proposed (called hereafter YBD) in order to describe the evolution of the structure as cations (Na) atoms are added to the melt and the mechanism of creation of non-bridging oxygens. This evolution is usually parameterized in terms of two ratios $K = [SiO_2]/[B_2O_3]$ and $R = [Na_2O]/[B_2O_3]$ ([.] indicate mol%). Using only the quantities K and R, the YBD model assumes that the borosilicate glasses contain several larger structural units like diborate, pyroborate, boroxol rings, reedmergnerite, danburite, etc...[1]. These units (also called supra-structural units) are in turn composed of basic units, such as four-coordinated silicon, three- and four-coordinated borons, and within the model one divides the Na_2O-B_2O_3-SiO_2 ternary diagram into four compositional regions. For every com-

* present address: Université Européenne de Bretagne, INSA, FOTON, UMR 6082, 35708 Rennes
† simona.ispas@univ-montp2.fr
‡ walter.kob@univ-montp2.fr

positional domain, the YBD model predicts the fraction of three- and four-fold coordinated borons ($^{[3]}$B and $^{[4]}$B) among total boron concentration as well as the fraction of bridging oxygens.

Following up these early ^{11}B NMR studies, other techniques were employed to explore the distribution of the structural groups and the mixing of silicate and borate units: combined Raman and ^{11}B NMR [20], X-ray absorption near-edge structure (XANES) [21], infra-red (IR) [22], as well as ^{29}Si, ^{17}O and ^{11}B NMR [9]. Further significant progress in understanding how silicate structural units mix with the borate $^{[3]}$B and $^{[4]}$B units has been made during the last two decades, and this was the direct consequence of the technical advances in solid-state NMR experiments, with the emergence of high-resolution magic-angle spinning (MAS) and especially multiple-quantum magic-angle spinning NMR techniques. For example Stebbins and co-workers have reported results on the concentration of $^{[4]}$B units, and also made assignments of the various oxygen sites, namely the Si-O-Si, B-O-B, Si-O-B and [Si,B]-O-Na linkages [7, 23–26]. The evolution of the $^{[4]}$B fraction has in fact attracted much interest, and various experimental studies have predicted that this concentration decreases if the quench rate increases [7, 16, 27].

Experiments show that borosilicate liquids and glasses present non-linear changes of their macroscopic properties with varying composition, temperature and pressure, and present days computer simulations can provide valuable atomic-scale information on both structure and dynamics. For the particular case of oxide glasses and liquids, atomistic simulations have become a well established tool for getting insight into the processes taking place at the microscopic level, known to control then the macroscopic properties [28, 29]. While the physics and chemistry of pure liquid and glassy SiO_2 [28, 30, 31] and B_2O_3 [32–39], have been intensively studied using simulations, there are so far only few numerical studies dedicated to ternary sodium borosilicate. The majority of those studies rely on the use of effective potentials, i.e. a classical molecular dynamics (MD) approach. The very first one was reported thirty years ago by Soules and Varshenya [40], who used a pair potential and primarily studied the boron coordination changes when the composition changes. Then a decade ago, Gou et al. [41] examined again the structure of some sodium borosilicate glasses using a three-body effective potential, and concluded that there was a tendency for the borate network to separate from the silicate part together with an association of sodium with the former. Very recently, Kieu et al. [42] have proposed a class of pair-potentials dedicated to this ternary system, and included a dependence between fitting parameters and composition in order to better reproduce the structural and mechanical properties over a wide compositional range. This approach allowed to reproduce certain aspects of the so-called boron anomaly [1].

Although simulations with effective potentials can certainly give valuable insight into the structural and dynamical properties of glass-forming systems, it is far from evident that they give quantitatively good results for multi-component systems since usually no reliable potentials are available. Hence for such systems it is preferable to use *ab initio* simulations based on density functional theory since these can handle also more complex local atomic environments. However, since often the concentration of one species is rather low, and *ab initio* simulations become computationally very expensive if the system size is large (say several hundred atoms), there exist so far relatively few studies that used this approach [43–47]. For borosilicate glasses, the only *ab initio* investigation so far reported in the literature, is a study of the structural and energetic effects of sodium substitution by hydronium ions [48].

The goal of the present study, as well as of the companion paper [49], is therefore to use *ab initio* simulations to obtain insight into the structure and dynamics of a sodium-rich borosilicate liquid and glass as a function of temperature. The composition of our system is 3 Na_2O-B_2O_3-6 SiO_2 (called NBS hereafter), and is similar to the composition used in glass wool. Within the YBD terminology, the present composition corresponds to $R = 3$ and $K = 6$. From an experimental point of view, there exist quite a few studies on the present composition in that NMR, Raman, XANES, and XPS experiments have been reported more than 10 years ago [19–21, 23, 50], and very recently a neutron diffraction study has been done [51]. These experimental studies have focused on the structural features of the glassy state and in the following we will compare these results with ours. In addition we mention that compositions quite close to our NBS system have been investigated by IR [22] and NMR [9] experiments, while Yamashita et al. [52] have studied its thermodynamic properties, and, taking into account the contributions of the structural units, have built a model for computing the heat capacity. We thus will discuss our results also with respect to these studies.

The paper is organized as follows: In the next section we present the details of the simulations. Section III we will discuss the structural properties of the liquid, and in Sec. IV the dynamical ones. Finally we summarize the results in Sec. V. Whereas the present paper focuses on the liquid, the accompanying paper, to which we will refer to as Part II, is devoted to the structural, electronic and vibrational properties of the glass.

II. SIMULATION DETAILS

The *ab initio* MD simulations were done using the Vienna *ab initio* package (VASP) [53, 54]. The system we have considered has the composition 3 Na_2O-B_2O_3- 6 SiO_2 and we have used a cubic box containing 320 atoms (60 silicon, 180 oxygen, 60 sodium and 20 boron atoms) and periodic boundary conditions. The edge length of the box has been fixed to 15.97 Å, which corresponds to

the experimental NBS mass density of 2.51 g/cm^3 [55].

The electronic structure has been calculated by means of the Kohn-Sham (KS) formulation of the Density Functional Theory (DFT) [56, 57] using the generalized gradient approximation (GGA) and the PBEsol functional [58, 59]. The choice of the recently proposed PBEsol functional [59] to describe the electronic exchange and correlation is motivated by the fact that for equilibrium structures and vibrational spectra of extended systems it often gives better results than other GGA functionals [60]. The KS orbitals have been expanded in a plane wave basis at the Γ-point of the supercell of the systems and the electron-ion interaction has been described within the projector-augmented-wave formalism [61, 62]. The plane-wave basis set contained components with energies up to 600 eV.

In order to solve the KS equations, we have used the residual minimization method-direct inversion in the iterative space [53], and the electronic convergence criterion was fixed at $5{\cdot}10^{-7}$ eV. For the *ab initio* MD simulations, the time step for the motion of the ions was chosen to be 1 fs and a Nosé thermostat [63] was applied to control the temperature in the canonical ensemble (NVT). To determine the vibrational properties of the glass we have cooled the sample to zero temperature and then determined the local minimum of the potential energy. This structural relaxation was stopped once the x, y, $z-$ components of the forces acting on each atom were inferior than 10^{-3} eV/Å.

The results presented in the next sections have been obtained by averaging over 2 independent samples. To generate an initial configuration, we have used a random arrangement of atoms placed in the simulation box. Subsequently we started the *ab initio* MD simulations within the NVT ensemble at 4500 K. After equilibration at this temperature, we performed NVT simulations at 4 lower temperatures: 3700 K, 3000 K, 2500 K, and 2200 K. For the three highest T's we discarded the first 0.5 ps from the total length of the runs before we started to measure the observables of interest, whereas for the two lowest temperatures we removed the first 1.5 ps. The lengths of the trajectories considered in the following for studying the structural and dynamic properties of the liquid were 2 ps for 4500 K, 2.5 ps for 3700 K, 7 ps for 3000 K, 20 ps for 2500 K, and 30 ps for 2200 K. We note that, except for the lowest temperature, we stopped the NVT simulations once the mean squared displacement (MSD) of the slowest element -i.e. silicon - reached ≈ 10 Å^2, which we considered as sufficient to assure that all the species have reached the diffusive regime. Due to the computational cost, we stopped the simulation at 2200 K before this criterion had been fulfilled. At this T the MSD of silicon atoms reaches ≈ 5.2 Å^2 (see subsec. IV A and Fig. 10d). At each one of these temperatures, we have computed the pressure of the liquid and we found the following values (for decreasing T): 3.0 GPa, 2.9 GPa, 2.2 GPa, 2.0 GPa and 1.2 GPa. A graph of these pressures as a function of T shows that for $T \approx 750$ K the pressure vanishes, i.e. at a temperature which is close to the experimental value of the glass transition temperature. Therefore we can conclude that our simulation is indeed able to predict the experimental value for the density of the glass.

In order to study the structural properties of the glass at room temperature, we have generated 6 samples that had different thermal histories due to the variation of the quench rate as well as of the starting temperature of the quench. More precisely, we have generated these samples using a two-steps procedure: Four samples were obtained by firstly quenching equilibrium configurations from 3000 K to 2000 K, using a quench rate of 2×10^{14} K.s^{-1}, and subsequently with a higher rate of 1.7×10^{15} K.s^{-1} from 2000 K to 300 K. For the two other samples we used configurations at 2200 K and quenched them to 1200 K, and then followed the second faster quench down to 300 K, using a rate of 9×10^{14} K.s^{-1}. At 300 K, we annealed the samples for 2 ps using the NVT ensemble. For two samples this annealing was followed by a run in the NVE ensemble of duration 8 ps and 15 ps, respectively. We have found that within statistical fluctuations all these samples had the same structural properties and therefore we have averaged these properties over all six samples. The mean pressure of these glassy sample was around -0.04GPa, which shows that despite the fast quench rate, we recover the experimental pressure.

III. STRUCTURE

In this section, we will present and discuss the static properties of our NBS liquid samples at the various temperatures considered. In addition we will also present the corresponding properties of the glass, even if these will be discussed only in Part II.

A. Radial Pair Distribution Functions

In Figs. 1 and 2, we show the partial pair distribution functions (PDF) $g_{\alpha\beta}(r)$ for α, $\beta = \mathrm{Si, O, B, Na}$, defined by [64]:

$$g_{\alpha\beta}(r) = \frac{V}{N_\alpha(N_\beta - \delta_{\alpha\beta})} \left\langle \sum_{i=1}^{N_\alpha} \sum_{j=1}^{N_\beta} \frac{1}{4\pi r^2} \delta(r - |\vec{r}_i - \vec{r}_j|) \right\rangle \quad , \tag{1}$$

where $\langle\cdot\rangle$ represents the thermal average, V is the volume of the simulation box, N_α is the number of particles of species α, and $\delta_{\alpha\beta}$ is the Kronecker delta. We note that Figs. 1 and 2 as well as all figures discussed in this subsection shows simulation data for both liquid and glass at 300 K, but the glass features will be discussed in Ref. [49]. Also we mention that, for the sake of clarity, we show only the functions for 3 of the 5 temperatures we simulated.

To start, we point out the common feature of the 10 pair correlations shown in Figs. 1 and 2 that the most

pronounced $T-$dependence is observed in the first peak in that it sharpens when temperature is lowered. This reflects the changes in the local bonding of the structural units SiO_n and BO_n of the silicate and borate subnetworks (discussed below), as well as in their mutual connectivity which increases when T decreases. Concerning the position of the maximum of the first peak, we find basically no change for the Si-O and O-O pairs, located at 1.63 Å and 2.62 Å respectively (see Figs. 1a and d), and this is consistent with the high concentration of SiO_4 tetrahedra which is more than 60% even at 4500 K (see Fig. 3). However, one should recall that the present simulations have been carried out at fixed density, which, due to the presence of the strong covalent bonding characterizing the SiO_4 tetrahedron, makes it difficult to change the local structure in a significant manner.

In contrast to this, the location of the first peak in the B-O and Na-O pairs shifts to higher values (see Fig. 1c and d): For the B-O pair, the first peak is located at 1.34 Å at 4500 K, while at 2200 K it is at 1.38 Å. This shift is related to the changes in the B-O coordination, since with decreasing T the percentage of tetrahedral BO_4 units increases, and the mean B-O nearest-neighbor distance is larger in tetrahedral BO_4 coordination than in trigonal BO_3 coordination or in defect BO_2 coordination present at the highest temperatures (see next subsection). For the Na-O pair, the first peak position shifts from 2.17 Å at 4500 K to 2.24 Å at 2200 K, and this is consistent with the increasing network polymerization as it can be derived from the $T-$dependence of the fractions of oxygen species found in our liquids: Bridging oxygens (BO), non-bridging oxygens (NBO) as well as tricluster oxygens (TBO) (see next subsection). We recall that BO are oxygen atoms connected to two network cations (Si and B), the NBO are connected to only one network cation, while the defective TBO units are connected to three network cations.

In Fig. 2, we show the PDFs of the two network formers, Si and B, as well as their correlations with sodium atoms, and the Na-Na pair correlation. Cooling from 4500 K to 2200 K has the usual effect that the structural order at short and intermediate distances (i.e. for $r \leq 7-8$ Å) increases, i.e. the peaks and the minima become more pronounced. In particular we note that in this $T-$range the height of the first-nearest-neighbour peak changes by only $15-20\%$ for the sodium correlations (Figs. 2d, e, and f). If the temperature is lowered to 300 K, the resulting change in the PDF is more pronounced which shows that the Na atoms settle into their preferred local structure only at relatively low temperatures, in agreement with the high diffusion constant found for this species (see below). (The same effect is observed in the Na-O correlation, see Fig. 1c.)

Figure 2b shows that the first peak in the B-B correlation splits into two if T is lowered from 2200 K to room temperature with the first peak is located at around 2 Å. This effect is related to the high quench rate used

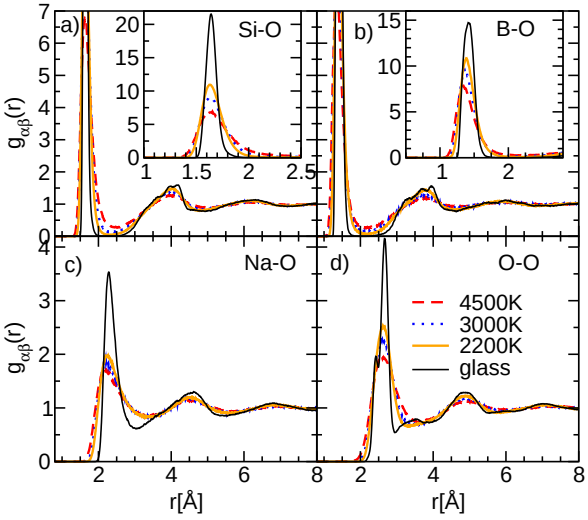

FIG. 1. Pair distribution functions for X-O pairs, (X = Si, O, Na, B) plotted for the liquid at three temperatures and the glass state at 300 K. The insets in the upper panels show the first peaks of the Si-O and B-O PDFs, respectively.

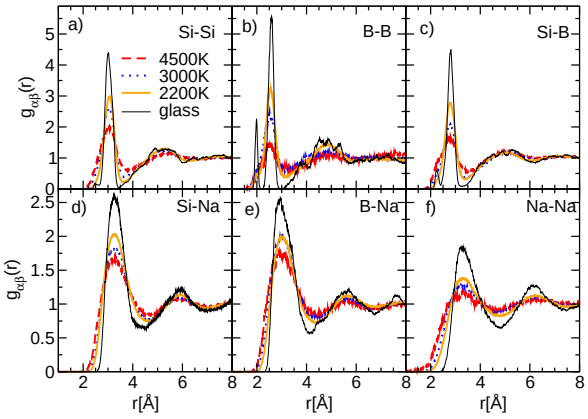

FIG. 2. Pair distribution functions $g_{\alpha\beta}(r)$ for α, β = Si, Na, B, plotted for the liquid at three temperatures and the glass state at 300 K.

in the simulations which freezes defective BO_n coordination polyhedra sharing also edges and not only corners. This B–B peak at small distances is also related to the presence of a sharp peak around 90° in the B–O–B bond angle distribution (see Fig. 9 below), since if one considers the average B-O distances in trigonal and tetrahedral borons (1.37 Å and 1.47Å, respectively) the resulting B–B distance is equal to 2 Å. Finally we note in panels a) and b) of Fig. 1 that for the glass the second nearest neighbor peak has several smaller peaks. The latter ones reflect the presence of SiO_n and BO_n coordination polyhedra ($n = 3, 4, 5, 6$) sharing not only corners but edges as well. Although the concentration of these defects decreases when temperature decreases (see below, and also Refs. [45, 65–67]), the involved distances become better defined and hence the corresponding peaks show up in

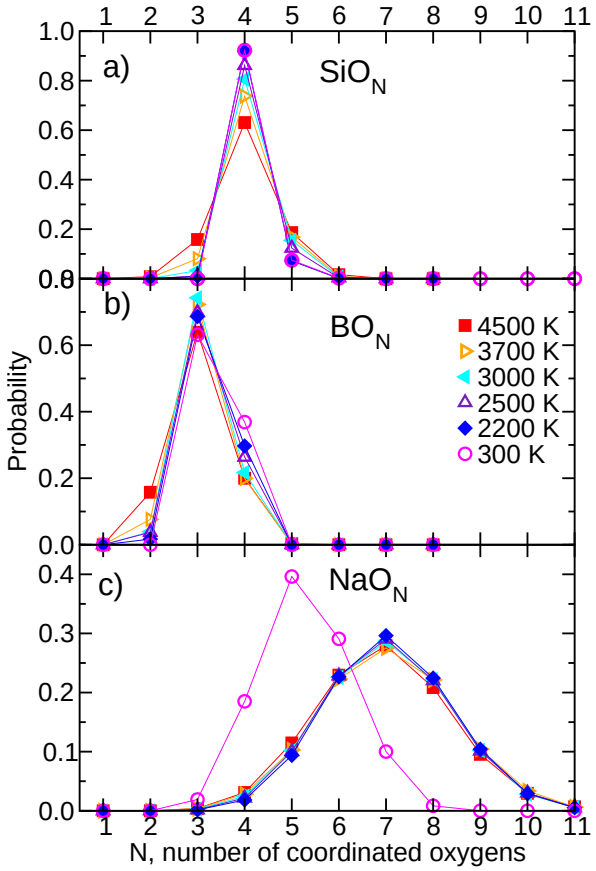

FIG. 3. Distributions of Si-O, Na-O and B-O coordinations for the liquid and glass at 300 K. The temperatures for the liquid are: 4500K, 3700K, 3000 K, 2500 K, and 2200 K.

the PDF only at low temperatures.

B. Coordination Numbers

A more detailed characterization of the local structure is given by the distribution of the coordination numbers. These distributions have been computed by defining two atoms to be nearest neighbours if their distance is less than the position of the first minimum of the corresponding PDF $g_{\alpha\beta}(r)$. Since we have found that this position is basically independent of temperature for the liquid, we have used the values 2.35 Å, 2.15 Å , and 3.40 Å for the Si-O, B-O and Na-O bond distance, respectively. For the glass state, we have used 2.0 Å for both Si-O and B-O bond distance, while a cutoff equal to 3.0 Å has been used for the Na-O coordination. Figure 3 shows the distributions of the oxygen coordinations with Si, Bi, and Na atoms for the five liquid temperatures as well as for the glass state.

For the Si-O coordination, shown in Fig. 3a, we find the expected trend, already reported for liquid silica or more complex silicate liquids [65, 66], that with decreasing temperature the percentages of defect units SiO_3 and SiO_5 decreases in favor of increasing of SiO_4 tetrahedral units. Hence at the highest temperature, one has 60% of Si atoms in a SiO_4 tetrahedral unit, while at 2200 K this percentage reaches 95%. We also note that, below 2500 K, there are no more under-coordinated SiO_3 units, and that, at the lowest liquid temperatures, the fraction of over-coordinated SiO_5 units is around 5% .

The distribution for the B-O coordination, shown in Fig. 3b, indicates that, at the highest T, one has around 20% BO_2 units and that cooling causes the gradual disappearance of this local structure in favor of formation of trigonal and tetrahedral borons. Since in the $T-$range 4500 K to 3000 K the concentration of BO_4 units is basically constant we can conclude that BO_2 is mainly converted into BO_3 units (see also Fig. 4a). For $T \leq 3000$ K the concentration of BO_2 units is less than 3%, and we note the conversion of trigonal borons to tetrahedral ones and at 2200 K the borate sub-network is essentially made up of BO_3 ($\approx$ 69%) and BO_4 ($\approx$ 29%) units. These changes in boron coordination with temperature are in qualitative agreement with the results of high temperature NMR experiments [7, 13, 15, 27, 68] for alkali borosilicates and boro-aluminosilicates. From these experiments it was concluded that the reaction BO_3+NBO $\rightarrow$ BO_4 takes place. However, if this would indeed be the main mechanism responsible for the conversion of BO_3 units into BO_4, the NBO concentration should decrease in the same manner as the increase of the BO_4 concentration, especially between 3000 K and 2200 K. Since this is not what happens for our system, as can be seen in Fig. 4a discussed below: The transformation of BO_3 units into BO_4 is more complicated than the above mentioned speciation reaction in that part of the transformation must involve a simultaneous change of the silicate sub-network.

The temperature dependence of the Na coordination number, shown in Fig. 3c, is somewhat surprising. For all the liquid states considered the distribution is basically independent of T, with most Na atoms having 6-8 neighbors. If, however, the samples are cooled to the glass state, this distribution shows a strong shift in that the new maximum is located at 5, with most Na atoms having between 4 and 7 neighbors. This very strong change is coherent with the results from the PDFs shown in Figs. 1 and 2 for which we found that these functions involving Na showed only a mild $T-$dependence in the liquid state but then changed quickly if the system is quenched into the glassy state.

Figure 4a shows the temperature dependence of the oxygen speciations (BO, NBO, and TBO, filled symbols), together with that of the boron units $^{[i]}$B, for $i = 2, 3, 4$, where i is the number of oxygen neighbors (open symbols). At the highest temperature, the TBO concentration is around 5%, and then decreases rapidly following basically an Arrhenius law, so that this species has almost disappeared at the lowest liquid temperature. From the figure we can also conclude that with decreasing temperature the network connectivity increases since the BO concentration increases quite quickly whereas the NBOs frac-

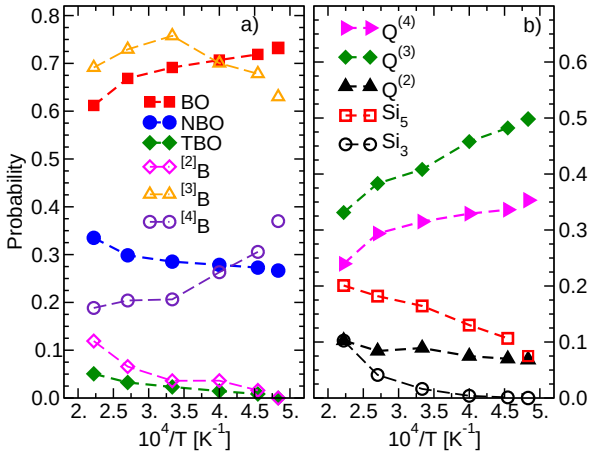

FIG. 4. Temperature dependence of the concentrations of BO, NBO and tricluster oxygen TBO, $^{[n]}$B for $n = 2, 3, 4$ (panel a), and of the $Q^{(n)}$ units for $n = 1, 2, 3, 4$ where $Q^{(n)}$ is a SiO_4 tetrahedron with n bridging oxygens for $n = 1, 2, 3, 4$, as well as of the defective units Si_5 and Si_3 (panel b). The symbols that are not connected by the lines correspond to the values for the glass state. Note that the two panels do not have the same scale on the ordinate.

tion is decreasing (and both $T-$dependencies are compatible with an Arrhenius law). If this $T-$dependence is extrapolated to 760 K, i.e. the experimental T_g, one finds a concentration of around 90% for BO and 10% for NBO, respectively. These values are not too far from the ones predicted by the YBD model (80% for BO and 20% for NBO) and also compatible with estimates from experiments [24].

Regarding the temperature dependence of the boron coordinations, the data plotted in Fig. 4a support the scenario mentioned above that $^{[2]}$B units are transformed into trigonal ones at the highest temperatures, since $^{[4]}$B is basically independent of T, followed by the conversion of $^{[4]}$B into tetrahedral units at lower temperatures. This reaction if probably only a first order approximation, since one can expect that there is also an interplay between the above mentioned changes and the ones related to the silicate sub-network, shown in Fig. 4b. Although in the temperature range in which we can equilibrate the liquid the majority of boron atoms is 3-fold coordinated, the $T-$dependence shown in Fig. 4a shows that this concentration is decreasing rapidly and that the one of $^{[4]}B$ is increasing. If one makes a reasonable extrapolation of this trend to the experimental glass transition temperature one predicts that at T_g the concentration of $^{[4]}$B is around 75% (and 25% $^{[3]}$B). For a more detailed discussion see Fig. 2 in Part II as well as the accompanying text.

For the silicate sub-network, a complementary information on its connectivity is given by the $T-$dependence of the $Q^{(i)}$ species, for $i = 2, 3, 4$, plotted in Fig. 4b, together with the percentages of 3-and 5-fold coordinated silicon atoms, denoted by Si_3 and Si_5, respectively. (We recall that $Q^{(i)}$ is a SiO_4 tetrahedron with exactly i bridging oxygens, and since there are almost no $Q^{(1)}$ units nor 6-fold coordinated Si, we do not show them.)

Firstly we note that the Si_3 concentration follows quite closely an Arrhenius law for decreasing temperatures and becomes basically zero at the lowest temperatures we have studied the liquid. Also the concentration of the Si_5 units decreases quite rapidly and a simple extrapolation to the experimental $T_g \approx 760$ K shows that at this temperature its concentration is also very close to zero. The $T-$dependence of the $Q^{(i)}$ species shows that the concentration of $Q^{(3)}$ increases rapidly, the one for $Q^{(4)}$ a bit slower, and the one for $Q^{(2)}$ decreases. In fact we find that the $T-$dependence of $Q^{(4)}$ cancels the one of Si_3 to a high accuracy (1% level) which suggests that if, with decreasing T, a 3-fold coordinated Si atom picks up an oxygen neighbor, it transforms into a $Q^{(4)}$ unit, i.e. it has no dangling oxygens. On the other hand, if a 5-fold coordinated Si atom sheds one of its oxygen neighbors, it will transform into a $Q^{(3)}$ unit (and to a smaller extent into a $Q^{(2)}$ unit). (This can be inferred from the fact that the sum of concentrations Si_3, $Q^{(3)}$, and $Q^{(2)}$ is only very weakly $T-$dependent.) This result is reasonable since it can be expected that the Si_5 unit was locally negatively charged and when it lost one oxygen it became a bit positively charged, thus impeding that the remaining oxygen atoms from bridging bonds. The oxygen freed by the Si_5 becomes now available to transform a $^{[3]}$B unit into a $^{[4]}$B. Thus we see that with this scenario the conversion of $^{[3]}$B into $^{[4]}$B is intimately linked to the T-dependence of the structure of the silicate sub-network.

C. Structure factors

The pair distribution functions are useful quantities to characterize the structure of a liquid at short distances. However, for intermediate and long distances it is better to consider their space Fourier transform, i.e. the partial structure factors. Figures 5 and 6 show the 10 partial structure factors characterising our liquid and glass, where $S_{\alpha\beta}(q)$ has been computed using the definition [64, 69]:

$$S_{\alpha\beta}(q) = \frac{f_{\alpha\beta}}{N} \sum_{j=1}^{N_\alpha} \sum_{k=1}^{N_\beta} \langle \exp(i\mathbf{q}.(\mathbf{r}_j - \mathbf{r}_k)) \rangle \quad \alpha, \beta = \mathrm{Si, O, Na, B}, \tag{2}$$

Here $f_{\alpha\beta} = 1$ for $\alpha = \beta$ and $f_{\alpha\beta} = 1/2$ otherwise and N is the total number of atoms.

As common features, we can firstly notice that each of the partial factors shows either a main peak or a negative dip for q vectors around 2.5-3.3 $\mathrm{\AA}^{-1}$, which reflects the local bonding inside the local structural units SiO_n and BO_n. The second characteristics is the presence of a less pronounced peak or negative dip at smaller wavevectors around $1.2 - 1.4\,\mathrm{\AA}^{-1}$, which is related to the

so-called first sharp diffraction peak (FSDP) and corresponds to the length scale associated to two connected SiO_4 tetrahedra [70, 71] and/or two trigonal boron units [37]. We note that the FSDP for the O-O pair is only a bump (see Fig. 5d), which indicates that the distribution of distances between two SiO_4 tetrahedra is broadened since the oxygen atoms can be connected either to Si or B atoms. For pure boron oxide liquid at 2500 K the *ab initio* molecular dynamics simulations by Ohmura and Shimojo [37] have shown the existence of pronounced peaks or a negative dip at 1.6 Å^{-1}, 2.4 Å^{-1} and 3.0 Å^{-1} for the three pair correlations B-O, O-O and B-B, and our corresponding NBS data present similar features, although slightly shifted due to the additional presence of Si and Na atoms. However, in our case the B-B correlation, Fig. 6c, these features are not very pronounced (note the scale in the graph) since in our composition the concentration of B_2O_3 is relatively low. Finally we point out that the Si-B correlation shown in Fig. 6b does not seem to go to zero for $q \to 0$ in the accessible q-range, which indicates the presence of a microphase separation of the two sub-networks. Previous classical MD simulations have indeed mentioned the tendency that the borate network separates from the silicate part together with an association of sodium with the former [41]. But this conclusion was rather qualitative as it was based only on snapshots of the system. Instead here we find that this trend is indeed observable in a correlation function.

Concerning the sodium correlations (see S_{NaO} in Fig. 5c, as well as S_{NaNa}, S_{SiNa}, and S_{NaB} in Fig. 6d, e, and f respectively), we note that they show a characteristic feature at about $1.3 - 1.4$ Å^{-1} for all considered temperatures: a shoulder for S_{NaNa}, and a negative dip for the three other correlations. In analogy to binary sodosilicate liquids [72–74], we can interpret this feature as indication for the presence of sodium rich channels in the structure, thus concluding that such intermediate range structures exist also in multicomponent glass-formers.

¿From the partial structure factors one obtains immediately the total static structure factors which can be compared to experimental results if available. We first consider the neutron structure factor, which is a linear combination of the partial structure factors [64]:

$$S_{\text{N}}(q) = \frac{N}{\sum_{\alpha=\text{Si,O,B,Na}} N_\alpha b_\alpha^2} \sum_{\alpha,\beta=\text{Si,O,B,Na}} b_\alpha b_\beta S_{\alpha\beta}(q) \tag{3}$$

with the neutron scattering length b_α given by $b_{\text{Si}} = 4.1491$ fm, $b_{\text{O}} = 5.803$ fm, $b_{\text{B}} = 6.65$ fm, and $b_{\text{Na}} = 3.63$ fm, respectively [75]. In Fig. 7 we present $S_{\text{N}}(q)$ for the liquid and glass states together with recent experimental results for the melt at 1273 K and the glass [51]. From Fig. 7 we can conclude that in general there is a rather good agreement between the results from the simulations and the experimental data. Several features can be noted: Firstly, there is a main peak around 5.0 Å^{-1} which becomes more pronounced and slightly shifts to higher q with decreasing temperature in both experimental and simulation data. Note that although this peak is the highest one in $S_{\text{N}}(q)$, it does not really correspond to a particular feature in the partial structure factors, hence making the interpretation of $S_{\text{N}}(q)$ rather difficult if one does not have access to the partials structure factors. Secondly both experimental and simulation data present a peak around 2.8-3.0 Å^{-1}, with a slight lower intensity for the simulation curves. This peak originates from the peaks present in almost all the partial structure factors in the same $q-$range and reflects the local bonding inside the structural units SiO_n and BO_n. The peak position and intensity seem to be basically independent of temperature although the partial structure factors do show a significant $T-$dependence (see Figs. 5 and 6). Concerning the features at small q (peaks around 1 Å^{-1} and 2 Å^{-1}) we see that they are significantly less pronounced than in the partial factors shown in Figs. 5 and 6, thus indicating the difficulty to observe them in a neutron scattering experiment.

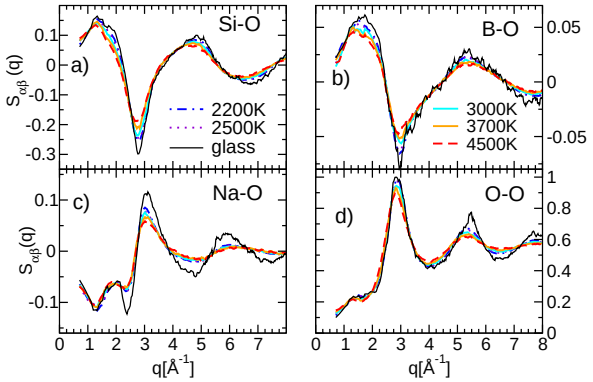

FIG. 5. Partial structure factors for liquid and glassy NBS, of X-O pairs, for X=Si, B, Na, and O. Note that the different panels do not have the same scale on the ordinate.

A further quantity which can be obtained from the partial structure factors and which is experimentally accessible is the X-ray total structure factor $S_X(q)$ which is given by [76]:

$$S_{\text{X}}(q) = \frac{N}{\sum_\alpha N_\alpha f_\alpha^2(q/4\pi)} \sum_{\alpha,\beta} f_\alpha(q/4\pi) f_\beta(q/4\pi) S_{\alpha\beta}(q)\,. \tag{4}$$

Here $f_\alpha(s)$ is the scattering-factor function (also called form factor), computed as a linear combination of five Gaussians using the parameters derived by Waasmaier and Kirfel [77]. The $q-$ dependence of $S_{\text{X}}(q)$ is shown in Fig. 8. In contrast to the neutron total structure factor, the X-ray total structure factor shows a pronounced peak around $2.1 - 2.3$ Å^{-1} and then a second one around $4.5 - 4.7$ Å^{-1}. When temperature is lowered, the first peak gains in intensity and its position shifts to smaller q, while the second peak only increases its intensity. The shoulder seen in $S_{\text{N}}(q)$ around 1.2–1.4 Å^{-1} is hardly vis-

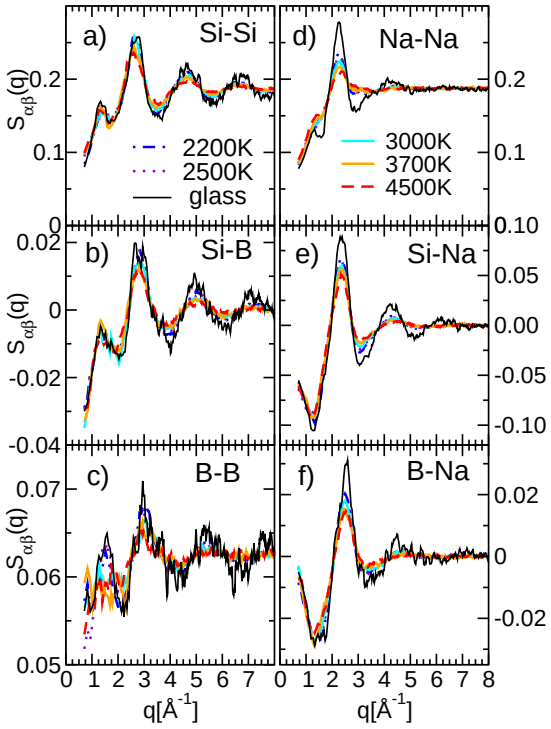

FIG. 6. Partial structure factors $S_{\alpha\beta}(q)$ for $\alpha, \beta =$ Si, B, Na. Note that the different panels do not have the same scale on the ordinate.

ible in $S_{\rm X}(q)$ so that one can conclude that, in experiments, the channel-like structure can be detected more easily by means of neutron scattering instead of X-ray scattering. As it is the case for $S_{\rm N}(q)$, we notice that the various peaks in $S_{\rm X}(q)$ are difficult to interpret since they are sum of too many partials.

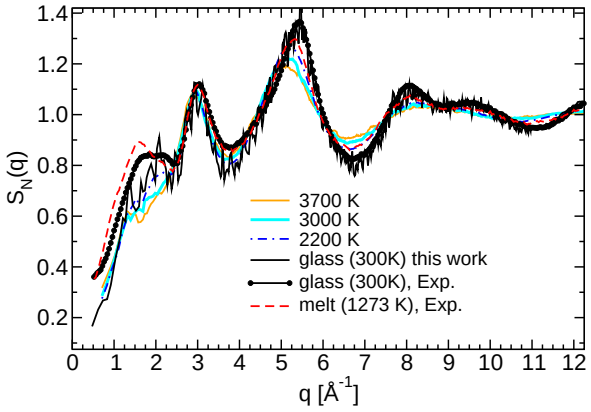

FIG. 7. Calculated and experimental neutron structure factor $S_N(q)$ for liquid and glass states. The experimental curves are from Ref. [51]

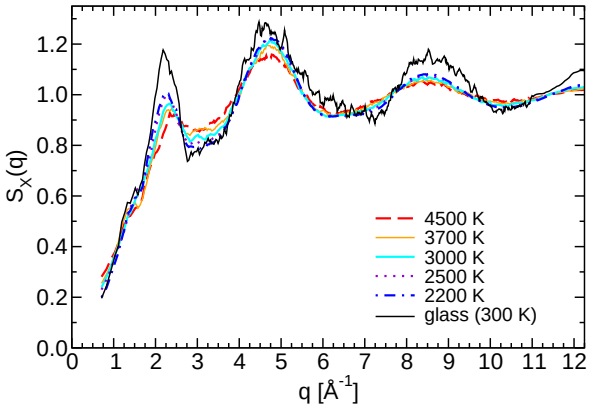

FIG. 8. Calculated X-ray structure factor $S_X(q)$ for liquid and glass states.

D. Bond Angle Distributions (BAD)

In order to get insight into the local connectivity within and between the local building blocks of the network, we have determined the distribution functions $P_{\alpha\beta\gamma}(\theta)$ of the bond angle formed by the triplet $\alpha-\beta-\gamma$. Among all possible combinations of triplets, we show in Fig. 9 the 3 sub-sets O$-\alpha-$O, $\alpha-$O$-\alpha$ and $\alpha-$O$-\beta$ for α, $\beta =$ Si, B, Na. As usual one finds that the distributions become more narrow if temperature is decreased. For the intra-tetrahedral angle OSiO, Fig. 9a, the distribution is quite broad at the highest temperature reflecting the presence of 3-, 5- and 6-fold coordinated Si, as well as distorted SiO_4 tetrahedra with NBOs. If T is lowered, we notice a slight shift of its maximum to higher angles and the formation of a small peak at 90° which corresponds to the presence of 5-fold coordinated Si.

Regarding the OBO angle, i.e. the intra-coordination polyhedron of the other network-former, Fig. 9b shows that the distribution is Gaussian-like for the liquid, but becomes split once the glass state is reached. In Part II [49], we will discuss the decomposition of this distribution for the glass into a contribution coming from the trigonal BO_3 units and tetrahedral BO_4 units.

The distribution $P_{\rm ONaO}$, Fig. 9c, is very broad, and one recognize two contributions: One at 60°, and a second one quite asymmetric around 90° with a long tail towards larger angles. For the NBS glass, we will discuss the origin of this double peak shape, already reported in previous simulations for low-silica alkali-alkaline earth melts [78] in Sec. II.B of the companion paper [49]).

For the so-called inter-tetrahedral angle SiOSi, shown in Fig. 9d, we have at 4500 K a broad distribution and when cooling to the lowest liquid temperature, its widths reduce significantly. At 2200 K, the function $P_{\rm SiOSi}$ shows a maximum around 130°, but also a shoulder around 90°. The latter is due to the presence of edge-sharing tetrahedra, as has been seen in other simulations of more simple silicates [45, 65, 67]. The BOB distribution, Fig. 9e, shows almost no $T-$dependence between 4500 K and

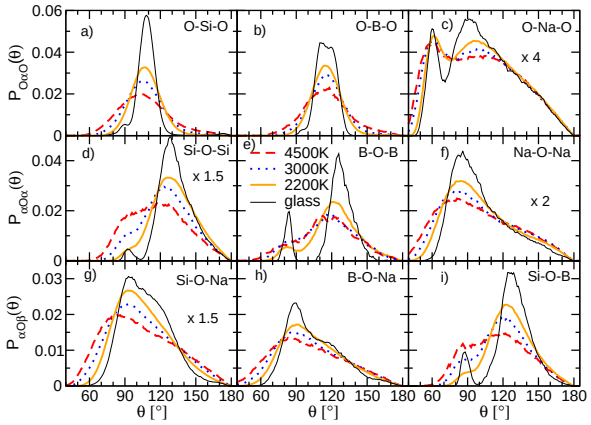

FIG. 9. Angular distribution functions $P_{\mathrm{O}\alpha\mathrm{O}}(\theta)$, $P_{\alpha\mathrm{O}\alpha}(\theta)$, and $P_{\alpha\mathrm{O}\beta}(\theta)$ for α, β, = Si, B, and Na shown for 3 temperatures in the liquid as well as for the glassy state. Distributions in panels c), d), f) and g) have been multiplied by the factor given in the panel in order to enhance their visibilities.

3000 K and is very broad, but once one has reached 2200 K one recognizes the presence of a shoulder at around 85°, which is related to BO_3 and BO_4 units that share an edge, and a pronounced peak around 125°. Note that at low T the distribution for SiOSi and BOB are qualitatively similar, which shows the similar role played by the network formers. However, we also recognize that B leads to significantly more edge sharing units than Si.

The last distribution involving the connectivity between two network-former units is the one for SiOB, shown in Fig. 9i. One sees that it is qualitatively similar to the distribution P_{SiOSi} and also the different peaks can be interpreted in an analogous manner.

For the distribution P_{NaONa}, shown in Fig. 9f, decreasing temperature affects both its width and maximum position in that it narrows and shifts to slightly higher angles, respectively. For the last two functions P_{SiONa} and P_{BONa}, see panels g and h in Fig. 9, we see that lowering T leads to a significant decrease of the probability at large angles. As it will be discussed in Ref. [49] this decrease is related to the fact that Na is avoiding the direction of the Si-O bond (or B-O bond).

IV. DYNAMICAL PROPERTIES

In the previous subsections we have discussed the structural properties of the liquid as a function of temperature. In the following we will concentrate on the dynamical features of the system. In particular we will present the mean squared displacement of a tagged particle, the van Hove correlation function, as well as the intermediate scattering function and discuss how these dynamical quantities are related to the structural ones.

A. Mean squared displacement and diffusion constant

The mean squared displacement (MSD) of a tagged particle of type α, $\alpha = \{\mathrm{Na}, \mathrm{O}, \mathrm{B}, \mathrm{Si}\}$ is given by [64, 69]:

$$r_\alpha^2(t) = \frac{1}{N_\alpha}\sum_{i=1}^{N_\alpha}\langle|\vec{r}_i(t) - \vec{r}_i(0)|^2\rangle. \qquad (5)$$

In Fig. 10 we show the time dependence of the MSD for the four atomic species in a double logarithmic plot. In agreement with previous results for the MSD of glass-forming systems [43, 45, 67, 70, 78–83] we find at short times a ballistic regime, i.e. $r_\alpha^2(t) \propto t^2$, and at long times the diffusion behavior, $r_\alpha^2(t) \propto t$. The fact that, for all temperatures considered, the MSD at long times shows a diffusive behavior is evidence that the runs are sufficiently long to fully equilibrate the system. Note that the time at which the ballistic regime ends depends on the species and hence also the value of the MSD that is reached at this crossover time depends on α. This shows that the mean free path for the particles, or the size of their cage at low temperatures, does depend on the species. In particular we find that for the Na atoms this size is significantly larger than the one for the other species.

The curves for the sodium atoms show that the ballistic regime is almost immediately followed by the diffusive regime which implies that even at the lowest temperatures this species does not experience a significant caging. This is in contrast to the behavior of the other types of atoms for which one finds at intermediate time scales a relatively flat region in the MSD, i.e. that the atoms are temporarily trapped. Furthermore one sees that at low T the curves for Si and B show in this caging regime several shoulders. These are related to the rattling motion of the atoms inside their cage which is rather complex and involves several frequencies and length scales (related to the position in time and the value of the shoulders, respectively), in particular for the B atoms. The details of this vibrational motion will be discussed in Ref. [49] where we present the density of states of the glass.

¿From the MSD at long times and the Einstein relation we can obtain the self-diffusion constants:

$$D_\alpha = \lim_{t\to+\infty}\frac{r_\alpha^2(t)}{6t} \quad , \qquad (6)$$

and in Fig. 11 we show the $T-$dependence of D_α in an Arrhenius plot. This graph demonstrates that in the $T-$regime considered the Na atoms are diffusing significantly faster than the other species, i.e. their motion is decoupled from the one of the other species, a result that is expected in view of the similar behavior found in sodo-silicate melts [73]. The $T-$dependence is given by an Arrhenius law with an activation energy around 0.74 eV. This value is only slightly smaller that the one

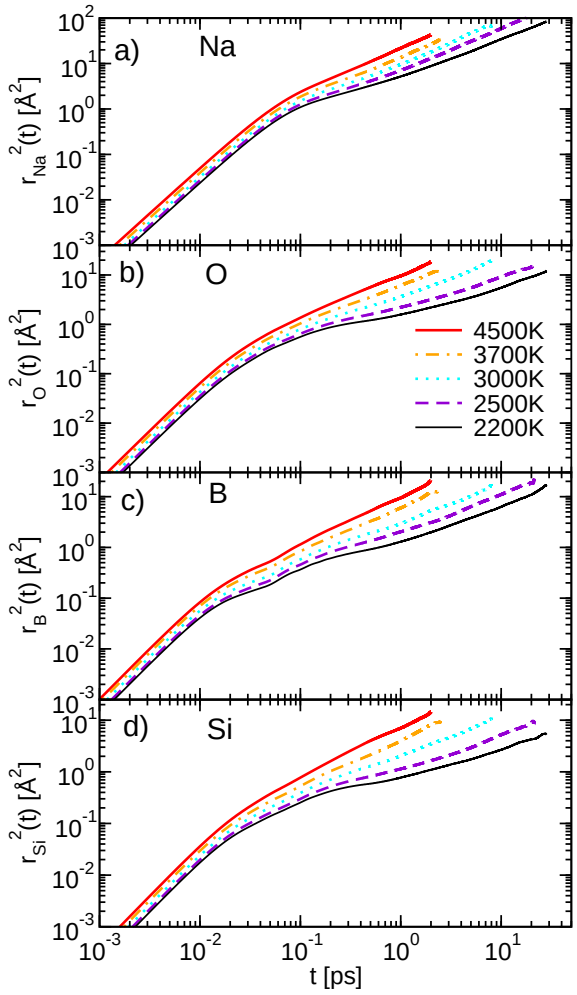

FIG. 10. Double logarithm plot of the mean squared displacement for Na (a), O (b), B (c), and Si (d) atoms, versus time for the five temperatures simulated.

reported from classical MD simulations for a sodium disilicate having a similar Na_2O concentration [82], which shows that these classical simulations give a fair estimate of the activation energy. Electrical conductivity experiments for sodium borosilicates that are rather boron rich have given, for temperatures above T_g, an activation energy between 1.4 and 2.2 eV whereas viscosity measurements give 0.65 and 0.85 eV [84]. For temperatures below T_g, Wu and coworkers [85, 86] have recently reported sodium tracer diffusion results, and extracted activation energies between 0.71 and 0.83 eV. Thus on overall we can conclude that the results from our simulation are compatible with the ones from experiments.

If we make the assumption that the Arrhenius law seen for Na holds also for temperatures down to the experimental glass-transition, i.e. 760 K, we can estimate that at T_g the diffusion constant of the Na atoms is around

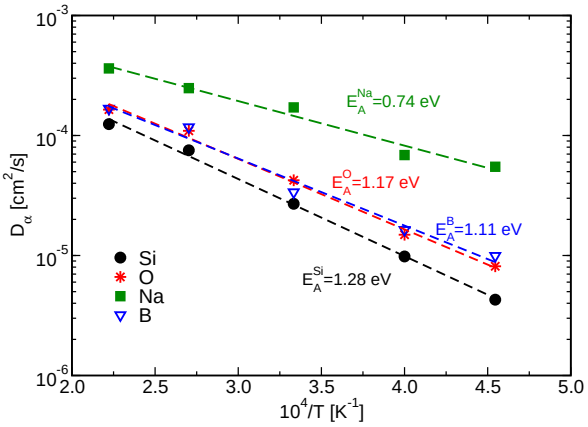

FIG. 11. Diffusion constants D_α for α = Na, O, B, and Si for the NBS liquid, plotted versus inverse temperature.

$8 \cdot 10^{-8}\mathrm{cm}^2/\mathrm{s}$, which is close to the experimental value reported for similar glass-formers [85, 86]. This shows that, although in our simulations we can access only relatively high temperatures, it is possible to extract also useful information at the experimental T_g.

In Fig. 10 we have seen that the motion for the Si atoms is the slowest one. The diffusion constant allows to make this statement more quantitative and from Fig. 11 we recognize that the corresponding diffusion constant is, at the lowest temperature considered, more than an order of magnitude smaller that the one for the sodium atoms. The $T-$dependence of D_{Si} is also given by an Arrhenius law and the activation energy is around 1.3eV, i.e. significantly larger than the one for the sodium atoms. We note, however, that this value for E_A^{Si} is by about a factor of four lower than the one found in pure silica [70, 87], which shows that the strong depolymerisation of the network does lead to much faster diffusion.

The diffusion constant for the oxygen atoms is a bit higher than the one of the silicon atoms in that the prefactor and the activation energy of the Arrhenius law are slightly larger. This result is in qualitative agreement with the behavior found in other silicate liquids and is related to the fact that for a diffusive step the oxygen has to break only one bond whereas a silicon atom has to break several ones.

Whereas the $T-$dependence of the diffusion constants for Na, Si, and O is not very surprising, the one for boron is: Although the role of this element is to be a network former and hence its dynamics should be slow, we find that D_{B} is within the numerical accuracy identical to D_{O}. Hence, despite the fact that a typical B atom is connected by three or four bonds to the matrix, it is still able to diffusive relatively quickly.

The result that boron diffuses faster than Si is in qualitative agreement with experiments on magmatic melts [88]. In these experiments the diffusion constant was determined from viscosity measurements at temperatures above T_g for a system that had a similar composition as the one considered here. However, in a different type of

experiment it has been reported that the activation energy for the viscosity is around 1.76 eV, i.e. significantly higher than the one obtained here [89]. Whether this difference is real or just due to the fact that diffusion constant and viscosity do not necessarily have the same activation energy (due to the breakdown of the Stokes-Einstein relation) remains open.

B. Van Hove correlation function

A more detailed understanding of the relaxation dynamics can be obtained from the self part of the van Hove function which is defined as [69]

$$G_s^\alpha(r,t) = \frac{1}{N_\alpha}\sum_{i=1}^{N_\alpha}\langle\delta(r-|\vec{r}_i(t)-\vec{r}_i(0)|)\rangle \quad \alpha \in \mathrm{Si, O, Na, B.} \tag{7}$$

Thus $G_s^\alpha(r,t)$ is the probability that in the time interval t a particle of type α has moved a distance r.

In Fig. 12, we show this function, multiplied by the phase space factor $4\pi r^2$, for the four species at 2200 K, at the following times: 0.0125ps, 0.025ps, 0.05ps, 0.1ps, 0.225ps, 0.45ps, 0.9ps, 1.9ps, 3.75ps, 7.5ps, 15ps, and 30ps.

Since at short times the atoms move ballistically, the self part of the van Hove function is just a Gaussian, which explains the peak of the curves seen in Fig. 12 for small t. For long times the particles diffuse and hence the distribution of their displacements is again a Gaussian. Thus the interesting information that can be obtained from $G_s(r,t)$ are the deviations from this Gaussian behavior. For high temperatures this Gaussian behavior is basically seen at all times and hence we focus here on the lowest temperature for which some deviations can be observed.

We see in Fig.12a that for the sodium atoms the distribution for $t = 1.9$ps and $t = 3.75$ps shows a weak shoulder at around $r = 3$. Since this distance corresponds to the nearest neighbor distance between two Na atoms (see Fig. 2f), we can conclude that on this time scale there is an increased probability (with respect to a purely diffusive process) that the atom which at $t = 0$ was at the origin has moved to this nearest neighbor distance. Such a behavior is the signature of a hopping-like motion, a type of movement which has been documented in previous classical simulations of sodo-silicate systems [82] but so far not within *ab initio* simulations.

For the oxygen and boron atoms we see that, at a given t, the distribution are more narrow than the one for the Na atoms, in agreement with the observation that the diffusion constants of O and B are smaller than the one for Na. For short and intermediate times the distributions do not show any particular feature. However, for the longest times one can notice a weak shoulder in $G_s(r,t)$ for oxygen at a distance around 3 Å, which is close to the nearest neighbor distance between two oxygen atoms. Also for boron one see a peak at around 2.5 Å and a second one at around 5 Å, i.e. the distances corresponding to the first and second nearest neighbor in the B-B correlation. Hence we can conclude that also boron has the tendency to make a hopping-like motion.

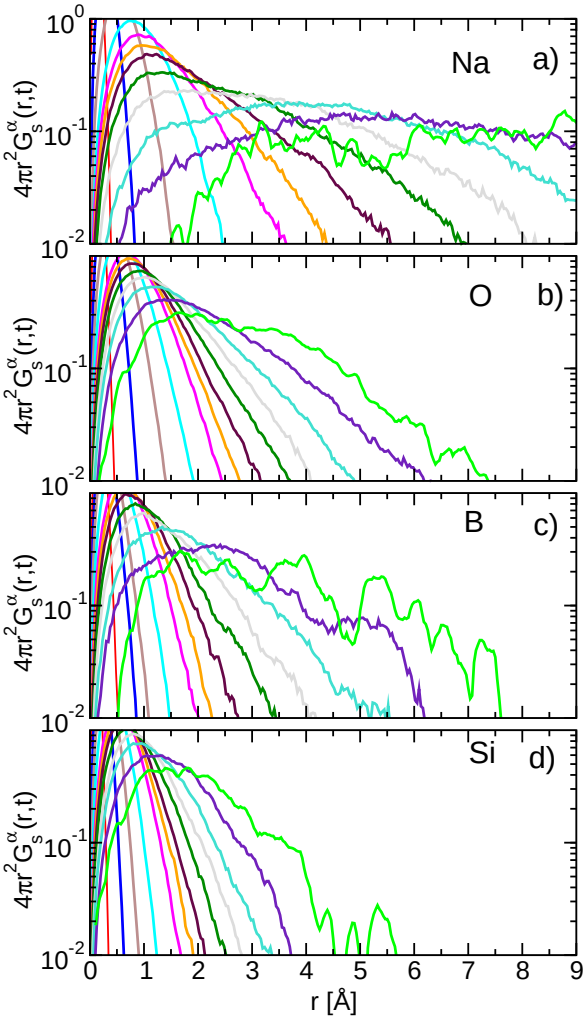

FIG. 12. The space dependence of the self-part of the van Hove correlation function $G_s^\alpha(r,t)$ for α =Na, O, B, and Si, at 2200K and for different times. The rightmost (green) curve corresponds to t =30 ps, and then from right to left the times are t = 15 ps, 7.5 ps, 3.75 ps, 1.9 ps, 0.9 ps, 0.45 ps, 0.225 ps, 0.1 ps, 0.05 ps, 0.025 ps and 0.0125 ps.

For silicon the distributions are the most narrow ones (see Fig. 12d), in agreement with the fact that the diffusion constant for silicon is the smallest one. We see that at the two largest times also this distribution shows a small shoulder at round $r = 3$ Å, i.e. the nearest neighbor distance between two Si atoms.

Finally we mention that if one plots $G_s(r,t)$, i.e. without the phase space factor $4\pi r^2$, one finds that at intermediate times, 0.5 ps $\leq t \leq$ 2 ps, and distances

$r \geq 1$ Å the distributions are described well by an exponential law (not shown). In the past such a behavior has been found also in other glass-forming systems (although less complex ones) and it has been argued that this feature is related to the fact that for short times the hopping motion of the particles do not yet follow the central limit theorem [90]. From our results we thus can conclude that the same mechanism is at work also in this rather complex glass-former.

C. Self intermediate function

The dynamical quantities we have discussed so far, the MSD and $G_s(r,t)$, are defined in real space. Although this makes the interpretation of the observables easy, they are not accessible in a real experiment of atomic systems, since scattering techniques probe the dynamics of the system in reciprocal space. It is therefore important to understand how the relaxation dynamics of our system would be seen in a scattering experiment. Furthermore we have so far discussed only the time dependence of single particles observables, which does not allow to make any conclusion on the nature of the collective relaxation motion. In order to address these points we will in the following discuss the time dependence of the coherent and incoherent intermediate scattering functions.

The incoherent intermediate scattering function $F_s(q,T)$ is defined as [69]

$$F_s^\alpha(q,t) = N_\alpha^{-1} \sum_{j=1}^{N_\alpha} \exp[i\vec{q}\cdot(\vec{r}_j(t) - \vec{r}_j(0))] \quad . \qquad (8)$$

Here $\vec{q}$ is the wave-vector and q its modulus. In Fig. 13 we show the time dependence of $F_s(q,t)$ and in order to improve the statistics we have averaged the correlator over wave-vectors in the range 1.05 Å$\leq q \leq$1.45 Å. Thus these $q-$values are the ones for which we have in the partial structure factors a pre-peak which is related to the presence of the channel-like structure of the Na atoms (see Fig. 7), i.e we are looking at the dynamics on length scales around 6 Å. We mention, however, that qualitatively similar results have been obtained also for other wave-vectors. as long as q is relatively small.

Figure 13 shows that at high T's the relaxation is quick and that the correlators show basically an exponential decay with relaxation times that are essentially independent of the species. In contrast to this the correlators show at low temperatures a two step decay, i.e. one sees at intermediate times a shoulder. This feature is directly related to the relaxation dynamics inside the cage [64]. We point out that also the correlator for Na does show a weak shoulder, thus giving evidence that even this species is somewhat caged, at least on this length scale. Although at low T the curves for the different species look qualitatively similar, we recognize that the $\alpha-$relaxation

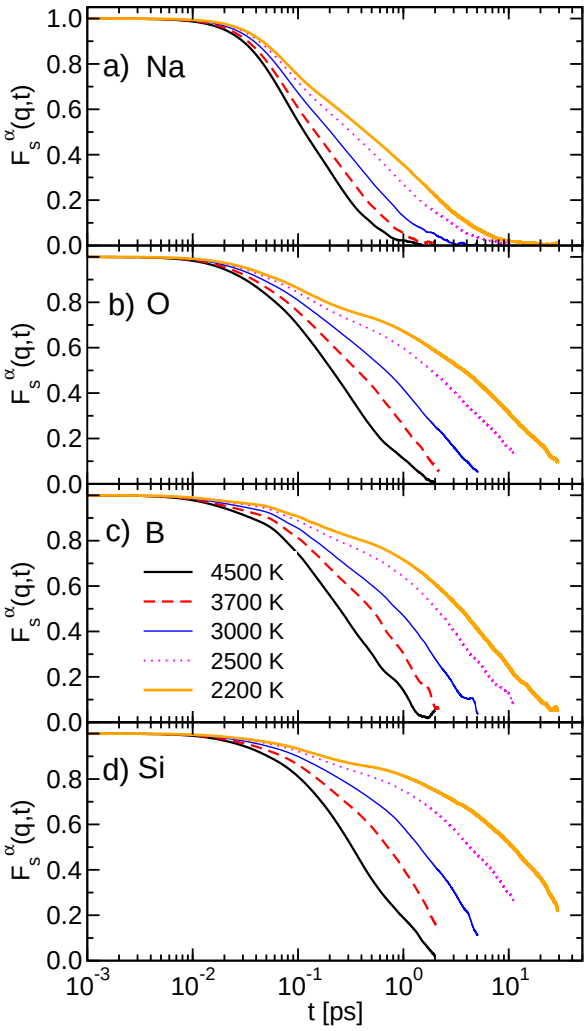

FIG. 13. The time dependence of the incoherent intermediate scattering function $F_s^\alpha(q,t)$ for α =Na, O, B, and Si, for the five temperatures simulated. The wave-vector has been averaged over the range 1.05 Å$^{-1} \leq q \leq$1.45 Å^{-1} in order to improve the statistics.

times are very different, in agreement with the strong species-dependence of the diffusion constant.

In Fig. 14 we show the time dependence of the coherent intermediate scattering function $F(q,t)$ defined as [69]

$$F_{\alpha\beta}(q,t) = f_{\alpha\beta} N_\alpha^{-1} \sum_{j=1}^{N_\alpha} \sum_{l=1}^{N_\beta} \exp[i\vec{q}\cdot(\vec{r}_j(t) - \vec{r}_l(0))] \quad . \qquad (9)$$

Here the factor $f_{\alpha\beta}$ is 0.5 for $\alpha \neq \beta$ and 1.0 for $\alpha = \beta$. A comparison of the curves in Fig. 13 with the one in Fig. 14 shows that for Si, O, and B the correlators are very similar in that their shape and relaxation time are basically the same, and this holds for all T. This is the usual behavior found in glass-forming liquids in that typically the self and collective functions decay on the same time scale. We see, however, that the sodium atoms

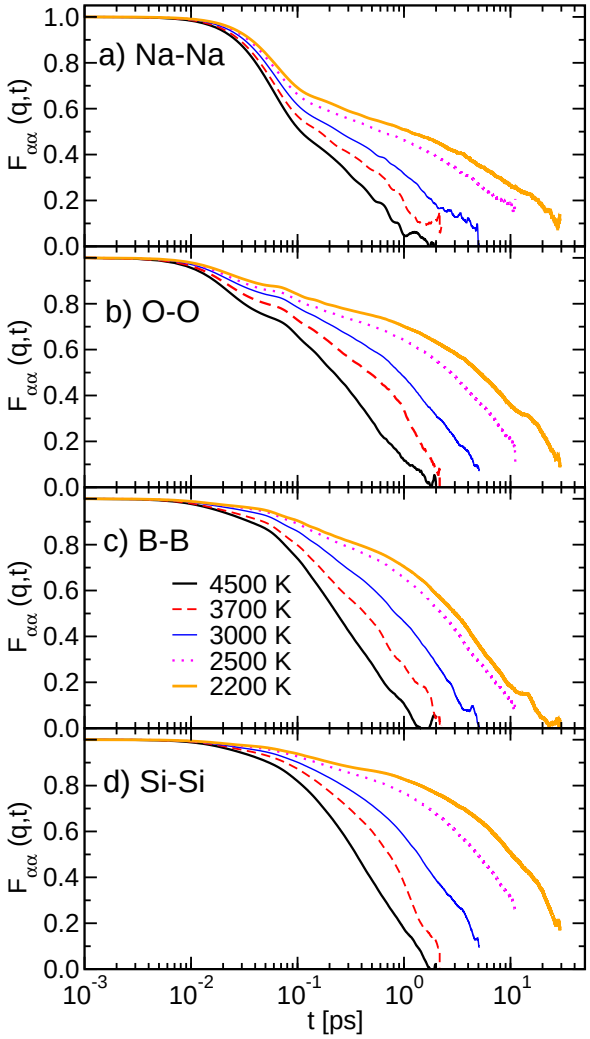

FIG. 14. The time dependence of the coherent intermediate scattering function $F_{\alpha\alpha}(q,t)$ for α =Na, O, B, and Si, for the five temperatures simulated. The wave-vector has been averaged over the range 1.05 Å^{-1} $\leq q \leq$1.45 Å^{-1} in order to improve the statistics.

do not follow this trend at all. Whereas the self function decays rather quickly, the collective function decays on the same time scale as the one for the other species. This clearly shows that in this system the Na atoms do have sites that are favorable: Even if an atom stays only for a short time at a given site (as can be concludes from $F_s^{\rm Na}(q,t)$), a vacated site is quickly occupied by another Na atom. The time scale to decorrelate the position of these "special sites" are therefore the ones it takes the matrix to rearrange, i.e. is given by the motion of the Si and O atoms. This result is in agreement with the one found in sodo-silicate glass-formers in which a strong decoupling of the coherent and incoherent correlator of the network modifier has already been documented [73]

V. SUMMARY

In this study, we have carried out first principles simulations for a ternary sodium borosilicate liquid and glass, with a chemical composition that is close to the one of glass wool. We have investigated the local and intermediate range order structural features in the liquid state with particular focus on how boron is embedded in the silicate network. We have found that in the liquid state the radial distribution functions, as well as the partial structure factors that involve Na, show a significantly smaller $T-$dependence than the ones of the network formers. Furthermore we find that the partial structure factors show at around 1.2 Å^{-1} a pre-peak which we see as evidence for the existence of channel like structures than have been observed in sodo-silicate systems before. However, our calculated X-ray and neutron structure factor shows that with these type of experiments it is difficult to see this pre-peak (with a slightly better chance for neutron scattering). The function $S_{\rm SiB}(q)$ does not seem to go to zero even at the smallest wave-vectors accessible in our simulations. This implies that these two network formers undergo a microphase separation on the scale of a few nanometers.

Special attention has been given to the boron coordination, found to be both trigonal and tetrahedral as expected for this composition. We have found that for the temperatures at which we have been able to equilibrate the liquid 60% of boron is threefold coordinated and 40% is fourfold coordinated. However, the $T-$dependence of these concentrations clearly shows that at the experimental glass transition temperature one expects this ratio to be very different, with the concentration of $^{[4]}$B reaching 70%.

Regarding the dynamics we have determined the mean squared displacements for all type of atoms and from them the diffusion constants. For all species we find that D_α is given by an Arrhenius law with activation energies that differ by a factor of 2 between Na and Si and which are in reasonable good agreement with experimental values determined at significantly lower temperatures. Surprisingly we find that the diffusion constant of boron is very similar to the one for oxygen (and significantly higher than the one of silicon). Thus for this system one of the network-formers is significantly more mobile than the other one.

The space and time dependence of the self van Hove functions shows that the Na atoms move, at the lowest temperatures, in a hopping-like manner. Although a bit less pronounced we find the same behavior for the boron atoms whereas the silicon atoms show a relaxation dynamics that is much more flow-like. Hence we see that these two network formers have a relaxation dynamics that differs not only quantitatively from each other but also qualitatively.

Finally we have also determined the time dependence of the coherent intermediate scattering function. We find that the ones for Si, O, and B are very similar to the one

for the incoherent functions, the one for Na is very different from $F_s^{\mathrm{Na}}(q,t)$. In particular we see that the former decays significantly slower than the latter, which is again evidence that individual sodium atoms are moving in a channel-like structure which relaxes only very slowly, i.e. on the time scale of the rearrangement of the matrix.

ACKNOWLEDGMENTS

We thank D. R. Neuville and B. Hehlen for stimulating discussions on this work. Financial support from the Agence Nationale de la Recherche under project POSTRE is acknowledged. This work was performed using HPC resources from GENCI (TGCC/CINES/IDRIS) (Grants x2010095045, x2011095045 and x2012095045), and also on the HPC@LR cluster, Montpellier, France. W. Kob acknowledges support from the Institut Universitaire de France.

[1] A. Varshneya, *Fundamentals of inorganic glasses, 2nd edition* (Society of Glass Technology, 2006)
[2] G. N. Greaves and S. Sen, Adv. in Physics **56**, 1 (2007)
[3] L. Trotignon, J. C. Petit, G. Della Mea, and J. C. Dran, J. Nucl. Materials **190**, 228 (1992)
[4] I. Bardez, D. Caurant, J. L. Dussossoy, C. Gervais, F. Ribot, D. R. Neuville, N. Baffier, and C. Fillet, Nuclear Science and Eng. **153**, 272 (2006)
[5] D. A. McKeown, A. C. Buechele, C. Viragh, and I. L. Pegg, J. Nucl. Materials **399**, 13 (2010)
[6] J. M. Delaye, S. Peuget, G. Bureau, and G. Calas, J. Non-Cryst. Solids **357**, 2763 (2011)
[7] S. Sen, Z. Xu, and J. F. Stebbins, J. Non-Cryst. Solids **226**, 29 (1998)
[8] S. Sen, J. Non-Cryst. Solids **253**, 84 (1999)
[9] R. Martens and W. Müller-Warmuth, J. Non-Cryst. Solids **265**, 167 (2000)
[10] L.-S. Du and J. F. Stebbins, J. Non-Cryst. Solids **315**, 239 (2003)
[11] D. Chen, H. Miyoshi, H. Masui, T. Akai, and T. Yazawa, J. Non-Cryst. Solids **345 - 346**, 104 (2004)
[12] L.-S. Du, J. Allwardt, B. Schmidt, and J. Stebbins, J. Non-Cryst. Solids **337**, 196 (2004)
[13] J. F. Stebbins, Chem. Geol. **256**, 80 (2008)
[14] D. Manara, A. Grandjean, and D. R. Neuville, J. Non-Cryst. Solids **355**, 2528 (2009)
[15] J. Wu, M. Potuzak, and J. F. Stebbins, J. Non-Cryst. Solids **357**, 3944 (2011)
[16] F. Angeli, O. Villain, S. Schuller, T. Charpentier, D. de Ligny, L. Bressel, and L. Wondraczek, Phys. Rev. B **85**, 054110 (2012)
[17] Y. Yun and P. Bray, J. Non-Cryst. Solids **27**, 363 (1978)
[18] Y. Yun, S. Feller, and P. Bray, J. Non-Cryst. Solids **33**, 273 (1979)
[19] W. Dell, P. Bray, and S. Xiao, J. Non-Cryst. Solids **58**, 1 (1983)
[20] B. C. Bunker, D. R. Tallant, R. J. Kirkpatrick, and G. L. Turner, Phys. Chem. Glasses **31**, 30 (1990)
[21] M. Fleet and S. Muthupari, J. Non-Cryst. Solids **255**, 233 (1999)
[22] E. I. Kamitsos, J. A. Kapoutsis, H. Jain, and C. H. Hsieh, J. Non-Cryst. Solids **171**, 31 (1994)
[23] S. Wang and J. F. Stebbins, J. Non-Cryst. Solids **231**, 286 (1998)
[24] S. Wang and J. F. Stebbins, J. Am. Ceram. Soc. **82**, 1519 (1999)
[25] S. K. Lee, C. B. Musgrave, P. Zhao, and J. F. Stebbins, J. Phys. Chem. B **105**, 12583 (2001)
[26] L.-S. Du and J. F. Stebbins, J. Phys. Chem. B **107**, 10063 (2003)
[27] J. Wu and J. F. Stebbins, J. Non-Cryst. Solids **356**, 2097 (2010)
[28] K. Binder, J. Horbach, A. Winkler, and W. Kob, Ceramics International **31**, 713 (2005)
[29] A. Tilocca, Proceedings of the Royal Society A: Mathematical, Physical and Engineering Science **465**, 1003 (2009)
[30] A. Pedone, J. Phys. Chem. C **113**, 20773 (2009)
[31] L. Giacomazzi, P. Umari, and A. Pasquarello, Phys. Rev. B **79**, 064202 (2009)
[32] A. Takada, C. R. A. Catlow, and G. D. Price, J. Phys.: Condens. Matt. **7**, 8659 (1995)
[33] A. Takada, C. Catlow, and G. Price, Journal of Physics: Condensed Matter **7**, 8693 (1995)
[34] P. Umari and A. Pasquarello, Phys. Rev. Lett. **95**, 137401 (2005)
[35] L. Huang and J. Kieffer, Phys. Rev. B **74**, 224107 (2006)
[36] G. Ferlat, T. Charpentier, A. P. Seitsonen, A. Takada, M. Lazzeri, L. Cormier, G. Calas, and F. Mauri, Phys. Rev. Lett. **101**, 065504 (2008)
[37] S. Ohmura and F. Shimojo, Phys. Rev. B **78**, 224206 (2008)
[38] S. Ohmura and F. Shimojo, Phys. Rev. B **80**, 020202 (2009)
[39] S. Ohmura and F. Shimojo, Phys. Rev. B **81**, 014208 (2010)
[40] T. F. Soules and A. K. Varshneya, J. Amer. Ceram. Soc. **64**, 145 (1981)
[41] F. Gou, G. Greaves, W. Smith, and R. Winter, J. Non-Cryst. Solids **293 - 295**, 539 (2001)
[42] L.-H. Kieu, J.-M. Delaye, L. Cormier, and C. Stolz, J. Non-Cryst. Solids **357**, 3313 (2011)
[43] P. Ganster, M. Benoit, W. Kob, and J.-M. Delaye, J. Chem. Phys. **120**, 10172 (2004)
[44] A. Tilocca and N. H. de Leeuw, J. Mater. Chem. **16**, 1950 (2006)
[45] J. Du and L. R. Corrales, J. Chem. Phys. **125**, 114702 (2006)
[46] S. Ispas, T. Charpentier, F. Mauri, and D. R. Neuville, Sol. St. Sciences **12**, 183 (2010)
[47] J. K. Christie, A. Pedone, M. C. Menziani, and A. Tilocca, J. Phys. Chem. B **115**, 2038 (2011)

[48] G. Geneste, F. Bouyer, and S. Gin, J. Non-Cryst. Solids **352**, 3147 (2006)
[49] L. Pedesseau, S. Ispas, and W. Kob, see accompanying paper(2014)
[50] Y. Miura, H. Kusano, T. Nanba, and S. Matsumoto, J. Non-Cryst. Solids **290**, 1 (2001)
[51] F. Michel, L. Cormier, P. Lombard, B. Beuneu, L. Galoisy, and G. Calas, J. Non-Cryst. Solids **379**, 169 (2013)
[52] I. Yamashita, T. Tojo, H. Kawaji, T. Atake, Y. Linard, and P. Richet, J. Chem. Thermodyn. **33**, 535 (2001)
[53] G. Kresse and J. Furthmüller, Phys. Rev. B **54**, 11169 (1996)
[54] G. Kresse and J. Furthmüller, Comp. Mat. Science **6**, 15 (1996)
[55] O. V. Mazurin, T. P. Shvaiko-Shvaikovskaya, and M. Streltsina, *Handbook of Glass Data: Ternary Silicate Glasses, Part C* (Elsevier Science Ltd, 1984)
[56] W. Kohn and L. J. Sham, Phys. Rev. **140**, A1133 (1965)
[57] R. Martin, *Electronic Stucture: Basic Theory and Practical Methods* (Cambridge University Press, 2004)
[58] J. P. Perdew, K. Burke, and M. Ernzerhof, Phys. Rev. Lett. **77**, 3865 (1996)
[59] J. P. Perdew, A. Ruzsinszky, G. I. Csonka, O. A. Vydrov, G. E. Scuseria, L. A. Constantin, X. Zhou, and K. Burke, Phys. Rev. Lett. **100**, 136406 (2008)
[60] R. Demichelis, B. Civalleri, M. Ferrabone, and R. Dovesi, Inter. J. Quant. Chem. **110**, 406 (2010)
[61] P. E. Blöchl, Phys. Rev. B **50**, 17953 (1994)
[62] G. Kresse and D. Joubert, Phys. Rev. B **59**, 1758 (1999)
[63] S. Nosé, Mol. Physics **52**, 255 (1984)
[64] K. Binder and W. Kob, *Glassy Materials and disordered solids* (Word Scientific, 2005)
[65] M. Benoit, S. Ispas, and M. E. Tuckerman, Phys. Rev. B **64**, 224205 (2001)
[66] S. Ispas, M. Benoit, P. Jund, and R. Jullien, J. Non-Cryst. Solids **307**, 946 (2002)
[67] M. Pöhlmann, M. Benoit, and W. Kob, Phys. Rev. B **70**, 184209 (2004)
[68] S. Sen, T. Topping, P. Yu, and R. E. Youngman, Phys. Rev. B **75**, 094203 (2007)
[69] J. P. Hansen and I. R. McDonald, *Theory of Simple Liquids* (Academic, London, 1986)
[70] J. Horbach and W. Kob, Phys. Rev. B **60**, 3169 (1999)
[71] J. Horbach, J. Phys.: Cond. Matter **20**, 244118 (2008)
[72] G. Greaves, J. Non-Cryst. Solids **71**, 203 (1985)
[73] J. Horbach, W. Kob, and K. Binder, Phys. Rev. Lett. **88**, 125502 (2002)
[74] A. Meyer, J. Horbach, W. Kob, F. Kargl, and H. Schober, Phys. Rev. Lett. **93**, 027801 (2004)
[75] `http://www.ncnr.nist.gov/resources/n-lengths/`
[76] H. E. Fischer, A. C. Barnes, and P. S. Salmon, Rep. Prog. Phys. **69**, 233 (2006)
[77] D. Waasmaier and A. Kirfel, Acta Crystallographica **A51**, 416 (1995)
[78] A. Tilocca, J. Chem. Phys. **133**, 014701 (2010)
[79] J. Sarnthein, A. Pasquarello, and R. Car, Phys. Rev. B **52**, 12690 (1995)
[80] M. Micoulaut, Y. Guissani, and B. Guillot, Phys. Rev. E **73**, 031504 (2006)
[81] M. Hawlitzky, J. Horbach, S. Ispas, M. Krack, and K. Binder, J. Phys.: Condens. Matt. **20**, 285106 (2008)
[82] J. Horbach, W. Kob, and K. Binder, Chemical Geology **174**, 87 (2001)
[83] A. Tilocca, Phys. Rev. B **76**, 224202 (2007)
[84] D. Ehrt and R. Keding, Phys. and Chem. of Glasses - European Journal of Glass Science and Technology Part B **50**, 165 (2008)
[85] X. Wu and R. Dieckmann, J. Non-Cryst. Solids **357**, 2846 (2011)
[86] X. Wu, A. K. Varshneya, and R. Dieckmann, J. Non-Cryst. Solids **357**, 3661 (2011)
[87] J. Mikkelsen, Appl. Phys. Lett. **45**, 1187 (1984)
[88] D. R. Baker, Geo. Cosmochim. Acta **56**, 617 (1992)
[89] B. Cochain, *Cinétique et mécanismes d'oxydo-réduction dans les silicates fondus*, Ph.D. thesis, Université Pierre et Marie Curie, Paris, France (2009)
[90] P. Chaudhuri, L. Berthier, and W. Kob, Phys. Rev. Lett. **99**, 060604 (2007)